

## Neutral H<sub>2</sub> and H<sub>2</sub><sup>+</sup> ions in the Saturnian magnetosphere

Wei-Ling Tseng,<sup>1</sup> Robert E. Johnson,<sup>1</sup> Michelle F. Thomsen,<sup>2</sup> Timothy A. Cassidy,<sup>3</sup> and Meredith K. Elrod<sup>1</sup>

Received 27 September 2010; revised 15 November 2010; accepted 27 December 2010; published 9 March 2011.

[1] The Saturnian system is immersed in an extended cloud of neutrals. Although water vapor ejected from Enceladus' south pole is the dominant neutral source, photolysis and radiolysis of ices can release H<sub>2</sub>O, O<sub>2</sub>, and H<sub>2</sub> from the icy ring particles and the icy satellites, and Titan's atmosphere is a source of H<sub>2</sub>. Once ionized, these neutrals are the source of the observed magnetospheric plasma. To understand the H<sub>2</sub><sup>+</sup> ion densities observed by the Cassini plasma spectrometer (CAPS), we developed a Monte Carlo test particle model to simulate the spatial morphology of the neutral H<sub>2</sub> cloud and the resulting H<sub>2</sub><sup>+</sup> ion source rates. The H<sub>2</sub> lifetime is constrained by its local chemistry, which is computed from the latest plasma measurements by Cassini CAPS data. The main rings, Enceladus' water torus, Rhea, and Titan are considered as the primary sources of H<sub>2</sub> in our model. It is seen that H<sub>2</sub> accumulates over Saturn's main rings because of thermal accommodation with the ring particles, and Titan is the dominant source of H<sub>2</sub> in the outer magnetosphere (>~6 R<sub>S</sub>). From ~6 to ~2.5 R<sub>S</sub>, photodissociation of water from Enceladus and H<sub>2</sub> scattered from the ring atmosphere are comparable sources. The newly formed H<sub>2</sub><sup>+</sup> ions are lost by collisions with the ring particles inside ~2.5 R<sub>S</sub>, by interchange processes in the middle magnetosphere, and by flow down the tail in the outer magnetosphere. The density distribution of H<sub>2</sub><sup>+</sup> estimated from our ion source rates roughly agrees with CAPS observations, and we show that the H<sub>2</sub><sup>+</sup> density near the equator over the main rings is at least 1 order of magnitude smaller than O<sub>2</sub><sup>+</sup>, possibly consistent with the nondetection of H<sub>2</sub><sup>+</sup> by CAPS at Saturn orbit insertion.

**Citation:** Tseng, W.-L., R. E. Johnson, M. F. Thomsen, T. A. Cassidy, and M. K. Elrod (2011), Neutral H<sub>2</sub> and H<sub>2</sub><sup>+</sup> ions in the Saturnian magnetosphere, *J. Geophys. Res.*, 116, A03209, doi:10.1029/2010JA016145.

### 1. Introduction

[2] The Voyager flyby measurements, HST observations and Cassini in situ observations have shown that the Saturnian system is immersed in a vast cloud of mostly water group neutrals [Broadfoot *et al.*, 1981; Shemansky and Hall, 1992; Shemansky *et al.*, 1993; Esposito *et al.*, 2005; Melin *et al.*, 2009]. Voyager also found a very broad distribution of the hydrogen atoms in a roughly doughnut-shaped cloud between 8 and 25 R<sub>S</sub> and with a vertical thickness of 14 R<sub>S</sub> [Broadfoot *et al.*, 1981]. After more complete data analysis of Voyager ultraviolet spectrometer observations, Shemansky and Hall [1992] indicated that the atomic hydrogen cloud in the Saturnian magnetosphere showed an azimuthal asymmetry dependent on local time with a slightly higher intensity on the dusk side. The upper atmosphere of Saturn is suggested to be

the source of H atoms due to the strongest emission appearing on Saturn itself [Shemansky and Hall, 1992; Shemansky *et al.*, 2009]. The first detection of an OH torus with a peak around 4 R<sub>S</sub> in the Saturnian system was obtained using Hubble Space Telescope [Shemansky *et al.*, 1993]. Modeling of the HST observations indicated that Enceladus and/or E ring icy grains were sources of the parent water molecules [Jurac *et al.*, 2002].

[3] The main rings, the icy satellites and Titan's escaping atmosphere are also important sources of neutrals and plasma in the Saturnian magnetosphere. Neutrals such as H<sub>2</sub>O, O<sub>2</sub> and H<sub>2</sub> are ejected from the rings and the icy satellites via incident UV photons, energetic plasma and meteorites, or via radiolytic decomposition of ice by photons and energetic particles. Most of the ejected neutrals escape from these icy objects but are still bound in Saturn's gravity, forming neutral tori, and orbiting Saturn until ionized. Once the neutrals are ionized, they are picked up and trapped in Saturn's magnetic field, producing a roughly toroidal source of magnetospheric plasma. Sputtering of the icy satellites and E ring was initially suggested as a source of the OH cloud observed using the Hubble Space Telescope [Shemansky *et al.*, 1993; Jurac *et al.*, 2002; Jurac and Richardson, 2005]. Although that modeling effort correctly estimated the size of the source and clearly indi-

<sup>1</sup>Materials Science and Engineering Department, University of Virginia, Charlottesville, Virginia, USA.

<sup>2</sup>Los Alamos National Laboratory, Los Alamos, New Mexico, USA.

<sup>3</sup>Jet Propulsion Laboratory, Pasadena, California, USA.

cated that the source of water molecules was primarily at the orbit of Enceladus, the exact nature of the source was not solved until the remarkable discovery by Cassini in 2005 that Enceladus was active [Waite *et al.*, 2006; Porco *et al.*, 2006; Hansen *et al.*, 2006].

[4] The large amount of molecules (water and its photodissociative products like OH, O and H) orbiting in the Saturnian system now appear to predominantly originate from Enceladus and are spread by charge exchange scatterings [Johnson *et al.*, 2006] and neutral-neutral collisions [Farmer, 2009; Cassidy and Johnson, 2010]. There are smaller contributions from other inner icy satellites and the icy particles in the tenuous E, F and G rings [Jurac *et al.*, 2001, 2002; Jurac and Richardson, 2005; Johnson *et al.*, 2008]. In particular Cassini plasma measurements showed a depletion in the energetic electrons in the vicinity of Rhea [Jones *et al.*, 2008] suggestive of radiolytic decomposition of Rhea's surface or its putative icy ring particles. The observed fluctuation in the spatial distribution of the O<sub>2</sub><sup>+</sup> ion density near Rhea's orbit appeared to be consistent with a source of neutral O<sub>2</sub> produced by radiolysis [Martens *et al.*, 2008]. Surprisingly, the main ring system was also found to be a significant source of O<sub>2</sub><sup>+</sup> [Waite *et al.*, 2005; Tokar *et al.*, 2005]. Since the high density of ring particles quenches the energetic particle flux, the oxygen molecules are primarily produced by the photolytic decomposition of ice. The neutral O<sub>2</sub> produced is subsequently ionized or scattered into the Saturnian magnetosphere [Ip, 2005; Johnson *et al.*, 2006; Tseng *et al.*, 2010]. Finally, Titan's exosphere is another major source contributing neutral H<sub>2</sub> and H, and smaller amounts of CH<sub>4</sub> and N<sub>2</sub>, although the rates for the later are still debated [Yelle *et al.*, 2008; Cui *et al.*, 2008; De La Haye *et al.*, 2007; Strobel, 2008; Tucker and Johnson, 2009; Johnson *et al.*, 2009].

[5] Thomsen *et al.* [2010] used Cassini plasma spectrometer and ion mass spectrometer (CAPS/IMS) data for a survey of plasma ion properties throughout the Saturnian magnetosphere. This survey is the first to address the densities and spatial distribution of the H<sub>2</sub><sup>+</sup> ions. Their results showed that a significant fraction of the ions in the outer magnetosphere are H<sub>2</sub><sup>+</sup> with a maximum in ratio of H<sub>2</sub><sup>+</sup> to H<sup>+</sup> near Titan's orbit, consistent with Titan as an important H<sub>2</sub> source in the outer magnetosphere. To understand the morphology of the H<sub>2</sub><sup>+</sup> ion torus observed by CAPS, in this work we investigate the possible neutral H<sub>2</sub> source rates and use these to simulate the spatial distribution of Saturn's H<sub>2</sub> cloud. Since one of the principal loss processes is ionization, we also provide the spatial morphology of the H<sub>2</sub><sup>+</sup> ion source rates. The main rings, Enceladus' water torus, Rhea and Titan are considered as the primary sources of H<sub>2</sub>. Each source rate is roughly estimated in this paper taking into account the photolytic reactions, electron impact dissociations and ionizations, and the ion-molecule collisions. The spatial variation of neutral H<sub>2</sub> lifetime is constructed using the Cassini CAPS plasma measurements, assuming azimuthal symmetry. A 3-D Monte Carlo model has been developed to simulate the density distribution of the neutral H<sub>2</sub> cloud. The final part of this work is to simulate the H<sub>2</sub><sup>+</sup> ion density distribution in the ionosphere of the main rings in an effort to account for the nondetection of H<sub>2</sub><sup>+</sup> over the main rings by Cassini

CAPS during Saturn orbit insertion (SOI) [Tokar *et al.*, 2005; Young *et al.*, 2005].

## 2. Model Description

### 2.1. Estimates of the H<sub>2</sub> Source Rates

#### 2.1.1. Main Rings

[6] Both neutral O<sub>2</sub> and H<sub>2</sub> molecules are released in a 1:2 ratio from icy ring particles and satellites' icy surfaces by decomposition by photons and energetic particles, processes referred to as photolysis and radiolysis, respectively [Johnson *et al.*, 1982; Johnson, 1990; Johnson *et al.*, 2004]. Although H<sub>2</sub>O is also ejected, its lifetime is short as it condenses out onto the low-temperature ring particles. Over the main rings, since most of the plasma is absorbed by the ring particles, neutral O<sub>2</sub> and H<sub>2</sub> were suggested to be produced by decomposition of ice by solar UV photons [Johnson *et al.*, 2006]. If the O<sub>2</sub> from ice decomposition is indeed the principal source of the O<sub>2</sub><sup>+</sup> ions observed by CAPS then there should be a corresponding source of H<sub>2</sub> and, hence, H<sub>2</sub><sup>+</sup>. The ejected H<sub>2</sub> and O<sub>2</sub> reimpact on the rings will not stick on the icy ring particles at expected temperature ( $T \sim 100$  K) and, hence, can accumulate in the atmosphere. Our work here focuses on the hydrogen component based on the previous detailed studies of the oxygen atmosphere [Ip, 1995, 2005; Johnson *et al.*, 2006; Luhmann *et al.*, 2006; Bouhram *et al.*, 2006; Tseng *et al.*, 2010]. Using the numerical model developed by Tseng *et al.* [2010], the neutral H<sub>2</sub> production rate is given as  $2 \times Q(\text{O}_2) \times (1 - f) \times A \times \cos \gamma$ , where  $A$  is the area of the rings and  $Q(\text{O}_2)$  is the flux of O<sub>2</sub> from the icy ring particles due to photolysis:  $Q(\text{O}_2) = 10^6 \text{ molecules cm}^{-2} \text{ s}^{-1}$  [Johnson *et al.*, 2006]. The UV flux on the sun-shaded side is modified by a factor of  $(1 - f)$ , where  $f$  is the fraction absorbed by the ring:  $f = \exp(-\tau/\cos \gamma)$ , which is determined by the optical thickness of the ring  $\tau$  and  $\gamma = 66.4^\circ$  is the incident angle of UV photons to the ring plane normal at the time Cassini passed over the rings (referred to as SOI). The above formula gives a net H<sub>2</sub> production rate  $\sim 2.0 \times 10^{26} \text{ s}^{-1}$  over the main rings at SOI. Since the H<sub>2</sub> desorbed from ice exhibits a quasi thermal distribution and returning H<sub>2</sub> thermally accommodates to the grain temperature, the spectra of ejected energies is assumed to be determined by the temperature of the ring particles [Johnson, 1990].

[7] There is an uncertainty in the H<sub>2</sub> source rate given above. As discussed by Ip [1995], Johnson *et al.* [2006] and Tseng *et al.* [2010], the recycling effect of O, O<sup>+</sup> and O<sub>2</sub><sup>+</sup> from photolytic fragments can recombine to form O<sub>2</sub> on icy ring particle surfaces. From their models, this effect could enhance the O<sub>2</sub> source rate by roughly a factor of 5–10. A factor of about 10 is also invoked to account for the CAPS data [Tokar *et al.*, 2005]. Although, the recycling effect of hydrogen (H, H<sup>+</sup> and H<sub>2</sub><sup>+</sup> → H<sub>2</sub>) could play the same important role for the H<sub>2</sub> source rate, the scale height of ring H<sub>2</sub> atmosphere is about 4 times that of O<sub>2</sub>. Therefore, the photolytic products of H<sub>2</sub> are more easily scattered from the main rings. There are, of course, other sources of hydrogen and oxygen for the ring system. Shemansky *et al.* [2009] and Melin *et al.* [2009] reported that there is a significant flux of H escaping from Saturn, a fraction of which could impact the rings. Water products from the Enceladus neutral torus could plate out on the A ring [Jurac and Richardson, 2007;

*Cassidy and Johnson*, 2010], possibly contributing to the neutral oxygen atmosphere [*Tseng and Ip*, 2011]. We will return to the recycling effect and its constraint by CAPS detection of O<sub>2</sub><sup>+</sup> as well as nondetection of H<sub>2</sub><sup>+</sup> in section 3.4.

### 2.1.2. Enceladus' H<sub>2</sub>O Torus

[8] The observation of Enceladus' active plumes ejecting water molecules and icy grains from its south polar region suggests that it is the dominant source of H<sub>2</sub>O, OH, and O in Saturn's inner magnetosphere [*Jurac et al.*, 2002; *Jurac and Richardson*, 2005; *Johnson et al.*, 2006; *Melin et al.*, 2009; *Smith et al.*, 2010; *Cassidy and Johnson*, 2010]. The broad OH torus detected by HST was suggested to be due to redistribution by charge exchange [*Johnson et al.*, 2006]. However, from the recent Cassini UVIS observations, *Melin et al.* [2009] obtained much broader distributions of the O and OH clouds than previous interpretations. In addition to charge exchange collisions and the energy release on molecular dissociation, the increased spreading is attributed to neutral-neutral collisions which take place in the densest part of the Enceladus' water cloud [*Farmer*, 2009; *Cassidy and Johnson*, 2010].

[9] We note that H<sub>2</sub> could also be a product of H<sub>2</sub>O molecules by photodissociation and electron impact dissociation to O + H<sub>2</sub>. Since *Smith et al.* [2010] indicated that photodissociation of H<sub>2</sub>O is the dominant dissociation process throughout the magnetosphere, we estimate the H<sub>2</sub> source rate from photodissociation of the water torus. Using the water cloud morphology from *Cassidy and Johnson* [2010], we find that  $\sim 3.5 \times 10^{34}$  H<sub>2</sub>O molecules are present in steady state produced by an average Enceladus' source rate of  $\sim 1 \times 10^{28}$  H<sub>2</sub>O s<sup>-1</sup> with a centrifugal scale height for neutrals,  $H_W \sim R_S \langle V_T \rangle / V_{\text{kepler}}(R_S)$ . It is  $\sim 10,000$  km at  $4.0 R_S$ , where  $\langle V_T \rangle = [8kT/\pi m]^{1/2} = 540$  m s<sup>-1</sup>. Using a photodissociation rate (H<sub>2</sub>O → H<sub>2</sub> + O) at  $\sim 1.1 \times 10^8$  s [*Huebner et al.*, 1992], in competition with charge exchange scattering from the system, ionization and dissociation to OH + H, we obtain a H<sub>2</sub> source rate of  $\sim 3 \times 10^{26}$  s<sup>-1</sup> from Enceladus' water cloud.

[10] The H<sub>2</sub> source rate depends, of course, on its parent H<sub>2</sub>O source rate from Enceladus, which has recently been shown to be highly variable. *Smith et al.* [2010] estimate values that range from  $1.1 \times 10^{27}$  H<sub>2</sub>O s<sup>-1</sup> to  $2.5 \times 10^{28}$  H<sub>2</sub>O s<sup>-1</sup> resulting in an uncertainty of a factor of 0.1–2.5 for our estimated H<sub>2</sub> source rate. To describe the fate of the H<sub>2</sub>, we use the updated Enceladus' water cloud distribution [*Cassidy and Johnson*, 2010] as the source location, and assume the orbital velocities of the H<sub>2</sub>O molecules are close to circular. Since photodissociation leads to an average excess energy of  $\sim 3.8$  eV with a peak at 3.2 eV [*Huebner et al.*, 1992], we assume each the H<sub>2</sub> receives  $\sim 2.8$  eV based on the mass ratio of the products.

### 2.1.3. Rhea

[11] Plasma-induced sputtering of the icy satellite surfaces and ice grains in the tenuous rings can contribute to the neutral clouds in Saturn's magnetosphere. *Johnson et al.* [2008] have evaluated the plasma ion sputtering rate of ice in Saturn's inner magnetosphere using the recent Cassini thermal plasma data [*Sittler et al.*, 2008] and new sputtering data for water ice [*Famá et al.*, 2008]. Multiplying their results of the globally averaged sputter flux for incident water group ions by the cross-section areas ( $\pi R^2$ ) of the icy

satellites, the H<sub>2</sub>O sputtering rate of the inner icy satellites is roughly estimated to be:  $\sim 4 \times 10^{24}$  H<sub>2</sub>O s<sup>-1</sup> for Enceladus,  $\sim 2.7 \times 10^{25}$  H<sub>2</sub>O s<sup>-1</sup> for Tethys,  $\sim 3 \times 10^{25}$  H<sub>2</sub>O s<sup>-1</sup> for Dione and  $\sim 9 \times 10^{24}$  H<sub>2</sub>O s<sup>-1</sup> for Rhea, respectively. These sputtering rates account for the total surface loss given in equivalent H<sub>2</sub>O, some of which is due to decomposition producing O<sub>2</sub> and H<sub>2</sub>. The fraction of O<sub>2</sub> and H<sub>2</sub> depends strongly on the ice temperature. From *Johnson et al.* [2008, equation (1)]: O<sub>2</sub> production is  $\sim 1.5\%$  at  $T = 80$  K and  $\sim 10\%$  at  $T = 100$  K. Assuming the average satellite surface temperature is  $T \sim 100$  K, and ignoring the surface area associated with the putative Rhea ring, the production rates from Rhea's surface are  $0.9 \times 10^{24}$  O<sub>2</sub> s<sup>-1</sup> and  $1.8 \times 10^{24}$  H<sub>2</sub> s<sup>-1</sup> (1:2 ratio).

[12] In addition, the decomposition due to the energy deposited by energetic ions and electrons must be included to estimate the total O<sub>2</sub> and H<sub>2</sub> source rates [e.g., *Johnson et al.*, 2004]. In the Saturnian magnetosphere, the thermal plasma is suggested to be predominantly formed by local ionization of neutrals inside Rhea's orbit, while the energetic plasma originating in the outer region diffuses into the inner magnetosphere via interchange with outward drifting cold plasma [*Hill et al.*, 2005; *Burch et al.*, 2005; *Rymer et al.*, 2007; *Schippers et al.*, 2008]. Since the maximum of the inwardly diffusing energetic electron flux occurs around Rhea's orbit [*Schippers et al.*, 2008] and Rhea has the largest surface area, this suggests that Rhea has the largest O<sub>2</sub> and H<sub>2</sub> source rates from radiolytic decomposition of ice by the energetic plasma ions and electrons.

[13] First we determine the energy deposition on Rhea's surface by the energetic plasma. For the energetic electrons, we use the sample measurements from Cassini CAPS and electron spectrometer (CAPS/ELS) and magnetospheric imaging instrument/low-energy magnetospheric measurement system (MIMI/LEMMS) which were published by *Schippers et al.* [2008]. Their data are well fit using two populations of electrons (thermal and suprathermal) each described by a kappa function. Using the kappa parameters at  $9.0 R_S$ , the energy deposition from magnetospheric electrons onto Rhea's surface (cross-section area:  $\pi R^2$ ) is estimated to be  $\sim 5.8 \times 10^{28}$  eV s<sup>-1</sup>. It is also found that the population of electrons with energies of hundreds eV to a few  $10^4$  eV makes the dominant contribution to energy deposition on Rhea. As for the energy deposition by energetic ( $>5$ – $10$  keV) H<sup>+</sup> and O<sup>+</sup>, we use the Cassini MIMI measurements published by *Dialynas et al.* [2009] to obtain  $\sim 5 \times 10^{26}$  eV s<sup>-1</sup> at  $9.0 R_S$ , which is much smaller than that due to the electrons. Although the efficiency of each of the types of radiation differs, we use here an average  $G$  value of 0.06 H<sub>2</sub> per 100 eV [*Johnson*, 2011; *Teolis et al.*, 2010] deposited in the ice except for energetic electrons ( $G$  value: the number of molecules produced for each 100 eV absorbed by a substance from ionizing radiation). For energetic electrons ( $>1,000$  eV), a  $G$  value of 0.006 H<sub>2</sub> per 100 eV is considered [*Johnson*, 2011; *Teolis et al.*, 2010]. The resulting H<sub>2</sub> source rate is roughly estimated to be  $\sim 4 \times 10^{24}$  s<sup>-1</sup> giving a total source rate of  $\sim 6 \times 10^{24}$  H<sub>2</sub> s<sup>-1</sup> including the sputtering component above. A summary of energy deposition into Rhea's surface by each plasma source is given in Table 1. As shown in Table 1, both sputtering from thermal magnetospheric O<sup>+</sup> and radiolysis from energetic electrons are important contributions to produce H<sub>2</sub>/O<sub>2</sub>. However, the

**Table 1.** A Summary of Energy Deposition on Rhea

Energy Source	Data Reference	Source Energy Range	Total Energy Deposit	H <sub>2</sub> Production Rate	G Value (per 100 eV)
MIMI O <sup>+</sup>	<i>Dialynas et al.</i> [2009]	9–677 keV	$3.2 \times 10^{25}$ eV/s	$1.9 \times 10^{22}$ /s	0.06
MIMI H <sup>+</sup>	<i>Dialynas et al.</i> [2009]	5.5–2300 keV	$4.6 \times 10^{26}$ eV/s	$2.8 \times 10^{23}$ /s	0.06
CAPS O <sup>+</sup>	<i>Johnson et al.</i> [2008]	–	–	$1.8 \times 10^{24}$ /s	–
CAPS H <sup>+</sup>	<i>Johnson et al.</i> [2008]	–	–	( $T_{\text{surface}} = 100$ K) $3.6 \times 10^{21}$ /s	–
Electron	<i>Schippers et al.</i> [2008]	1– $10^3$ eV	$1.1 \times 10^{27}$ eV/s	$6.6 \times 10^{23}$ /s	0.06
Electron	R1 flyby (A. Rymer, private communication, 2010)	$10^3$ – $10^6$ eV	$5.7 \times 10^{28}$ eV/s	$3.4 \times 10^{24}$ /s	0.006
Electron		$10^3$ eV– $4 \times 10^5$ eV	$6.8 \times 10^{27}$ eV/s	( $T_{\text{surface}} = 100$ K) $4.0 \times 10^{23}$ /s	0.006

energetic electron intensity is highly variable around Rhea’s orbit (A. Rymer, private communication, 2010). It is seen in Table 1 that the energetic electron flux during the first Rhea flyby in 2005 was roughly an order of magnitude smaller than the averaged value reported by *Schippers et al.* [2008] thus reducing the source rate. In addition, the energy deposition of the energetic O<sup>+</sup> (MIMI O<sup>+</sup> shown in Table 1) might be slightly underestimated since the “effective area” of absorption could be a few times larger than the cross-section area ( $\pi R^2$ ). *Pospieszalska and Johnson* [1989] showed that hot heavy ions could reach the leading hemisphere for some combination effects of pitch angle distribution and gyroradius. The contribution of H<sub>2</sub> from decomposition of Rhea’s putative icy dust rings is not included in present work and will be discussed in section 3.1.

#### 2.1.4. Titan

[14] Titan’s atmosphere is primarily composed of N<sub>2</sub> (>95%), CH<sub>4</sub> (~4%) and H<sub>2</sub> (~0.1%–0.2%) with trace elements of hydrocarbons. The Cassini INMS measurements suggested that Titan probably has a larger atmospheric loss rate than previously thought [*Yelle et al.*, 2008; *Cui et al.*, 2008; *De La Haye et al.*, 2007]. There are a number of theoretical and observational studies of the heating and of escape from Titan: *Cui et al.* [2008] (thermal escape), *De La Haye et al.* [2007] (chemical-induced escape), *Strobel* [2008] (slow hydrodynamic escape) and *Michael et al.* [2005] (atmospheric sputtering). Detailed discussions and a summary of sputtering and heating of Titan’s upper atmosphere are given by *Johnson* [2009] and *Johnson et al.* [2009]. Although the loss rates for CH<sub>4</sub> and N<sub>2</sub> are debated, there is a rough agreement for Titan’s H<sub>2</sub> escape rates

between pre-Cassini and Cassini estimates. *Cui et al.* [2008] studied the vertical distribution of H<sub>2</sub> from Titan based on Cassini INMS data, and suggested the thermal escape of H<sub>2</sub> at a rate  $\sim 1 \times 10^{28}$  s<sup>-1</sup>, which is comparable to the pre-Cassini estimates [*Lebonnois et al.*, 2003]. However, *Strobel* [2008] interpreted the INMS data using a hydrodynamic fluid model that included thermal conduction and solar heating, and inferred an H<sub>2</sub> escape rate a factor of two smaller than in the work of *Cui et al.* [2008]. The latest DSMC modeling done by *Tucker and Johnson* [2009] suggested no enhancement for mass loss due to heat conduction from exobase below. So in this work, we assume a thermal escape rate of  $1 \times 10^{28}$  H<sub>2</sub> s<sup>-1</sup> from Titan with a Maxwellian thermal velocity distribution at an exospheric temperature of  $T = 151$  K [*Cui et al.*, 2008]. A summary of each H<sub>2</sub> source, production mechanism and source rate is given in Table 2.

#### 2.2. H<sub>2</sub> Lifetime

[15] The H<sub>2</sub> lifetime is constrained not only by the magnetospheric plasma environment (ion/electron density and temperature) but also by the solar photon flux. The ion densities and temperatures of H<sup>+</sup> and W<sup>+</sup> (water group ions) in the Saturnian magnetosphere are taken from Cassini CAPS and RPWS measurements published by *Persoon et al.* [2009], *Wilson et al.* [2008] and *Sittler et al.* [2008]. *Schippers et al.* [2008] provided a survey of electron densities and temperatures near the equator throughout the magnetosphere. They showed that there are two principal components of electrons: the dense, relatively cold thermal component, with a peak at  $\sim 4$ – $5 R_S$ , and the tenuous rela-

**Table 2.** A Summary of H<sub>2</sub> Sources, Production Mechanisms, and Source Rates

Source	Production Mechanism	H <sub>2</sub> Production Rate <sup>b</sup> (s <sup>-1</sup> )
Main rings	Photolytic decomposition	$\sim 2 \times 10^{26}$ at SOI
	Maxwellian thermal velocity distribution at $T = 100$ K <sup>a</sup>	An enhanced factor of $\sim 10$ due to recycling <sup>b</sup>
Enceladus’ water torus	Photodissociation of H <sub>2</sub> O	$\sim 3.0 \times 10^{26}$
	Keplerian orbital velocity plus excess energy $\sim 2.84$ eV from photodissociation distributed in a random direction <sup>a</sup>	A factor of 0.1 to 2.5 due to variable Enceladus source rates <sup>b</sup>
Rhea	Radiolysis decomposition by energetic plasma	$\sim 6.1 \times 10^{24}$
	Maxwellian thermal flux distribution at $T = 100$ K <sup>a</sup>	A factor of 0.5 due to variable energetic plasma flux <sup>b</sup>
Titan	Thermal escape	$\sim 1.0 \times 10^{28}$
	Maxwellian thermal flux distribution at $T = 151$ K <sup>a</sup>	A factor of $\sim 2$ smaller with Strobel’s value <sup>b</sup>

<sup>a</sup>H<sub>2</sub> ejection velocity distribution.

<sup>b</sup>Uncertainty of H<sub>2</sub> production rate.

**Table 3.** Photolytic Reactions<sup>a</sup>

Reaction	Rate (s <sup>-1</sup> )
H <sub>2</sub> + hv → H + H	7.4 × 10 <sup>-10</sup>
H <sub>2</sub> + hv → H <sub>2</sub> <sup>+</sup> + e	9.2 × 10 <sup>-10</sup>
H <sub>2</sub> + hv → H + H <sup>+</sup> + e	2.0 × 10 <sup>-10</sup>

<sup>a</sup>Huebner et al. [1992].

tively hot suprathermal component, which peaks at ~9.0 R<sub>S</sub>. Since there is no latitudinal information on either electron component, we use the same variation of both populations with latitude by equating the electron density to the total ion density (sum of H<sup>+</sup> and W<sup>+</sup>).

[16] A chemistry network is developed involving the photodissociation/ionization, electron impact dissociation/ionization and ion-molecule reactions. Table 3 shows the photolytic ionization and dissociation rates at Saturn's orbit [Huebner et al., 1992]. The electron impact dissociation/ionization rate,  $\nu$ , is given by  $\nu = n_e \times \sigma(u) \times u$ , where  $u$  ( $=\sqrt{\pi kT/8m_e}$ ) is the average electron velocity for a given electron temperature given by Schippers et al. [2008],  $n_e$  is the electron number density and  $\sigma(u)$  is the energy-dependent electron impact cross section. As for the ion-molecule reaction rate  $\alpha$ , it is derived from  $\alpha = n_e \times \sigma(E_i) \times V_i$  with the relative ion-neutral collision speed  $V_i$ , the energy-dependent charge exchange cross section  $\sigma(E_i)$ , and the local ion density  $n_i$ . For simplicity, here we assume that collisional cross sections between neutral H<sub>2</sub> and water group ions (H<sub>3</sub>O<sup>+</sup>, H<sub>2</sub>O<sup>+</sup>, OH<sup>+</sup> and O<sup>+</sup>) are the same as that of O<sup>+</sup>. The electron impact reaction rates and charge exchange rates as a function of electron and ion energy are given in Tables 4 and 5, respectively. These are combined to compute the spatial variation of neutral H<sub>2</sub> lifetime in a two-dimensional Saturnian magnetosphere of azimuthally symmetry.

[17] Figure 1 shows the variation with distance from Saturn of the neutral H<sub>2</sub> lifetime at the equator. Over the main rings, H<sub>2</sub> has a very long lifetime ~6 × 10<sup>8</sup> s since the photolytic reactions dominate. The lifetime of H<sub>2</sub> is a minimum at ~9.0 R<sub>S</sub> which roughly coincides with peak in the electron impact ionization rate. This in turn is produced by a peak in the density and energy of the electrons at that distance [Schippers et al., 2008]. The charge exchange rate with the water group ions has its maximum at 4–6 R<sub>S</sub>.

## 2.3. Orbital Dynamics

### 2.3.1. A Model of the H<sub>2</sub> Cloud

[18] Following the same numerical approach developed by Tseng et al. [2010], we track test particles in three dimensions based on a Monte Carlo choice of emission from each source in order to describe the neutral H<sub>2</sub> cloud in the Saturnian magnetosphere. Test particle trajectory integra-

**Table 4.** Electron Impact Ionizations and Dissociation<sup>a</sup>

Reaction	Cross Section at Electron Energy 20 eV (10 <sup>-16</sup> cm <sup>2</sup> )	Cross Section at Electron Energy 200 eV (10 <sup>-16</sup> cm <sup>2</sup> )
H <sub>2</sub> + e → H + H	0.751	0.147 (at 80 eV)
H <sub>2</sub> + e → H <sub>2</sub> <sup>+</sup> + 2e	0.28	0.676
H <sub>2</sub> + e → H + H <sup>+</sup> + 2e	0.0086	0.0545

<sup>a</sup>Yoon et al. [2008].**Table 5.** Charge Exchange Reactions<sup>a</sup>

Reaction	Cross Section at Ion Energy 200 eV (10 <sup>-16</sup> cm <sup>2</sup> )	Cross Section at Ion Energy 2 keV (10 <sup>-16</sup> cm <sup>2</sup> )
H <sub>2</sub> + H <sup>+</sup> → H <sub>2</sub> <sup>+</sup> + H	0.563	7.37
H <sub>2</sub> + O <sup>+</sup> → H <sub>2</sub> <sup>+</sup> + O	8.36	3.71

<sup>a</sup>Tawara et al. [1985].

tions are done by a Runge-Kutta algorithm. The center of coordinate system is fixed at Saturn and Saturn's gravity is accounted for the equation of motion. The lifetime of neutral H<sub>2</sub> in the Saturnian system is limited by the local chemistry as discussed. In order to account for the loss of H<sub>2</sub>, the weight of each test particle is reduced by a value of  $\exp(-\Delta t/T_{\text{Loss}})$  in an integration time step ( $\Delta t$ ) where  $T_{\text{Loss}}$  is the local destruction time scale due to ionization, dissociation and charge exchange scattering as described above. The test particle trajectory integrations are terminated when the molecules are lost to Saturn or when they move outside a radial distance of 60 R<sub>S</sub>. When the corresponding weighting factor is less than 0.01 because of chemical loss or to ring absorption, the trajectory integration is also terminated. The neutrals and ions are coupled via ion-neutral collisions in the magnetosphere which play an important role in modifying their morphologies [Johnson et al., 2006; Cassidy and Johnson, 2010; Tseng et al., 2010]. The ion-neutral collisions will be discussed in section 2.3.2. In our modeling, the 3-D grid system is divided into 120 × 200 × 160 grid points with  $\Delta\theta = 3^\circ$ ,  $\Delta R = 0.2 R_S$  and  $\Delta Z = 0.1 R_S$ . The simulated density is converted into a real neutral H<sub>2</sub> density by multiplying by a factor,  $C = Q/(N/\Delta t)$  where  $Q$  is a H<sub>2</sub> production rate,  $N$  is the number of test particles, and  $\Delta t$  is an integration time in each step. The neutral H<sub>2</sub> density distribution from each source is simulated separately and the total cloud distribution is given by a sum.

[19] For the main ring source, H<sub>2</sub> is injected in a random direction from the ring plane with an initial weighting factor according to the ring optical thickness. The initial ejection

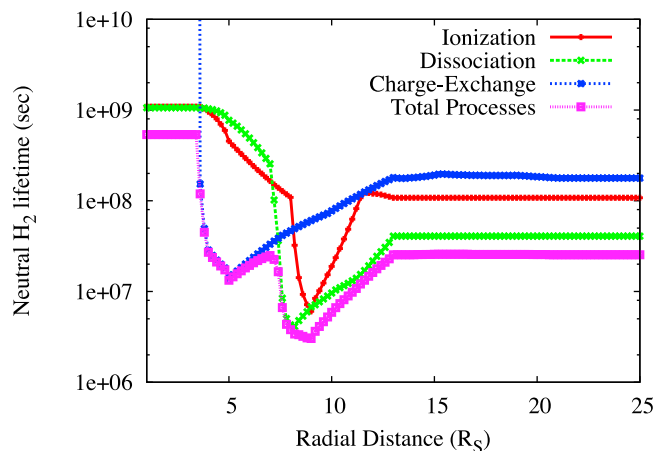


**Figure 1.** Neutral H<sub>2</sub> lifetime (in s) as a function of distance from Saturn (in unit of Saturn's radius, R<sub>S</sub>) at the equator. Lifetimes for ionization (red), dissociation (green), charge exchange (blue), and all processes combined (pink) by photolysis, electron impact, and charge exchange are accounted for.

velocity of an H<sub>2</sub> test particle is the local Keplerian velocity of the ring particle plus an ejection velocity in a random direction with a Maxwellian thermal velocity distribution at temperature  $\sim 100$  K. Like O<sub>2</sub>, the H<sub>2</sub> molecules do not permanently stick on the icy ring particles at low temperature  $\sim 100$  K. On impacting an icy ring particle the temporarily absorbed H<sub>2</sub> will accommodate to the ring particle temperature and be subsequently ejected with a Maxwellian velocity distribution according to the local temperature. The absorption probability of neutral H<sub>2</sub> by a ring particle is determined by  $P = 1 - \exp(-\tau/\cos \alpha)$ , where  $\tau$  is the optical depth at the point of impact and  $\alpha$  is the incident angle between the H<sub>2</sub> velocity in the rotating frame of the ring and the normal to the ring plane. The temporarily absorbed H<sub>2</sub> is then reemitted in a random direction with a Maxwellian distribution of velocities according to the local ring temperature.

[20] Each H<sub>2</sub> from dissociation of H<sub>2</sub>O in the Enceladus water torus is assigned with an initial weighting factor determined by the local water density modeled by *Cassidy and Johnson* [2010]. Each test particle is ejected randomly from the Enceladus water torus with local Keplerian velocity plus the photodissociation excess energy distributed in a random direction. H<sub>2</sub> would obtain an extra energy  $\sim 2.84$  eV from photodissociation of water (see section 2.1). As a consequence, the total H<sub>2</sub> velocity is close to Saturn's escape velocity at  $4 R_S$  ( $\sim 17.7$  km s<sup>-1</sup>) so that Enceladus' H<sub>2</sub> torus is highly dispersed in the magnetosphere.

[21] H<sub>2</sub> molecules which are ejected from Rhea, with an initially equal weighting factor, as a result of radiolysis decomposition of ice by energetic plasma are assumed to have a Maxwellian distribution based on the local T (=100) on the surface of Rhea with a exit angle ( $\theta$ ) distribution  $f(\theta) = \cos(\theta)$ . For Rhea's H<sub>2</sub> cloud, the three body equation of motion (test particle, satellite and planet) which is solved by rotating the coordinate system of the satellite [*Danby, 1989; Ip, 1997*] is taken into account in this model.

[22] Because Titan's orbital period is much shorter than the dynamical lifetime of H<sub>2</sub>, and we are not attempting to describe the atmosphere close to Titan's surface, the injection from Titan can be approximated by a ring of continuous distribution of emission points located at  $20.2 R_S$ . Therefore, H<sub>2</sub> is isotropically ejected, with an initially equal weighting factor, from Titan's orbit in equally spaced regions following a Maxwellian velocity distribution of an exospheric temperature at  $\sim 151$  K [*Cui et al., 2008*].

### 2.3.2. Ion-Molecule Collisions

[23] As mentioned in sections 1 and 2.1, a number of studies have shown that ion-molecule collisions in the main rings and in the inner magnetosphere are very important for redistributions of neutrals [*Johnson et al., 2006; Tseng et al., 2010; Cassidy and Johnson, 2010*]. The ion-molecule collisions are included in this model as the following: H<sub>2</sub> + H<sub>2</sub><sup>+</sup>, H<sub>2</sub> + O<sub>2</sub><sup>+</sup>, H<sub>2</sub> + W<sup>+</sup> and H<sub>2</sub><sup>+</sup> + O<sub>2</sub>. The charge exchange of H<sub>2</sub> + H<sub>2</sub><sup>+</sup>, H<sub>2</sub> + O<sub>2</sub><sup>+</sup> and H<sub>2</sub><sup>+</sup> + O<sub>2</sub> over the main rings is taken into consideration because we can simulate the H<sub>2</sub><sup>+</sup> ion density distribution over main rings as described in section 3. Over the main rings, since the ion-neutral collisional speeds are slow, scattering is nearly isotropic in the center of mass system [e.g., *Johnson et al., 2006*]. So, after a neutral H<sub>2</sub> collides with an H<sub>2</sub><sup>+</sup> ion or an O<sub>2</sub><sup>+</sup> ion, the outgoing velocity of each species in the inertial frame is the

initial velocity of the center of mass plus a velocity in a random direction that is equal to the relative collision speed scaled by a mass ratio. The H<sub>2</sub><sup>+</sup> ion density and velocity distribution over the main rings is modeled by treating the ion-molecule interactions iteratively. The charge exchange interaction of H<sub>2</sub> + H<sub>2</sub><sup>+</sup> is  $2.6 \times 10^{-10}$  cm<sup>3</sup> s<sup>-1</sup> as determined by the Langevin rate constant,  $2\pi[\alpha \times (Ze)^2/m]^{0.5}$  where  $\alpha$  is the polarizability of H<sub>2</sub> (=5.45) [*Johnson, 1981; Hasted, 1972*], and  $m$  is the reduced mass. The reaction rates of H<sub>2</sub> + O<sub>2</sub><sup>+</sup>  $\rightarrow$  H<sub>2</sub><sup>+</sup> + O<sub>2</sub><sup>\*</sup> ( $1.9 \times 10^{-10}$  cm<sup>3</sup> s<sup>-1</sup>) and O<sub>2</sub> + H<sub>2</sub><sup>+</sup>  $\rightarrow$  O<sub>2</sub> + H<sub>2</sub><sup>+</sup>\* is ( $\sim 2.1 \times 10^{-9}$  cm<sup>3</sup> s<sup>-1</sup>) are also determined by the polarizabilities of H<sub>2</sub> and O<sub>2</sub>, respectively, but with different reduced masses. The O<sub>2</sub> and O<sub>2</sub><sup>+</sup> density and velocity distributions are adopted from the simulated results of *Tseng et al.* [2010].

[24] In addition to the charge exchange interaction of H<sub>2</sub> + H<sub>2</sub><sup>+</sup> and H<sub>2</sub> + O<sub>2</sub><sup>+</sup> elastic scattering of H<sub>2</sub> by the water group ions must be included. The densities and temperatures of water group ions are taken from the CAPS data as described in section 2.2. As the relative speed between the ions and neutrals increases, the isotropic scattering gives way to forward scattering. So for collisions between H<sub>2</sub> and W<sup>+</sup>, the scattering angle ( $\chi$ ) in the center of mass system is calculated by the same procedure used by *Cassidy and Johnson* [2010]. To calculate the ion-neutral scattering angle, we use a differential scattering cross section approximated by  $dQ/d\Omega = (u^{-4/n})(1 - \cos(\chi))^{1(1+1/n)}$  with  $n = \infty$  where  $u$  is the relative collision speed [*Cassidy and Johnson, 2010, equation (1)*]. The total scattering cross section is  $\sigma_T(\chi_0) = \int_{\chi_0}^{\pi} (d\sigma/d\Omega)d\Omega$ , where  $\pi$  is the maximum scattering angle and  $\chi_0$  is the minimum scattering angle in the center of mass frame. Here,  $\chi_0$  is determined by  $\chi_0 = (\hbar \times 2 \times M \times \Delta l)/u \sim (14 \text{ m s}^{-1})/u$  where  $M$  is the reduced mass,  $\Delta l$  is one Bohr radius and  $u$  is the relative collision speed. Usually,  $\chi_0$  is very small because  $u$  is much larger than  $14 \text{ m s}^{-1}$ . A scattering angle  $\chi$  is then chosen via a Monte Carlo method from the formula  $\sigma_T(\chi)/\sigma_T(\chi_0) = R$ , where  $R$  is a random number between 0 and 1. For simplicity, the water group ions (W<sup>+</sup>) are again treated as O<sup>+</sup> ions. In order to account for elastic scattering, the total scattering rate is assumed to be two times the charge exchange rate of H<sub>2</sub> and O<sup>+</sup> [*Johnson, 1990*]. The average O<sup>+</sup> ion velocity is determined from the water group ion temperature distribution inferred from Cassini CAPS measurements [*Sittler et al., 2008; Wilson et al., 2008; Persoon et al., 2009*].

## 3. Results and Discussions

### 3.1. Spatial Distributions of Neutral H<sub>2</sub>

[25] Figure 2 (left) shows the spatial variations of the azimuthally averaged H<sub>2</sub> column density along the vertical height ( $Z$  direction) (number cm<sup>-2</sup>) of each source as a function of a distance from Saturn (in unit of Saturn's radius,  $R_S$ ). The equatorial H<sub>2</sub> number density of each source is also shown in Figure 2 (right). Obviously, Titan is a dominant source of H<sub>2</sub> in the magnetosphere outside  $\sim 6 R_S$  and is the largest source rate:  $\sim 1.0 \times 10^{28}$  s<sup>-1</sup> ( $\sim 2$  orders of magnitude larger than other sources as seen in Table 2). This supports result of the CAPS plasma survey made by

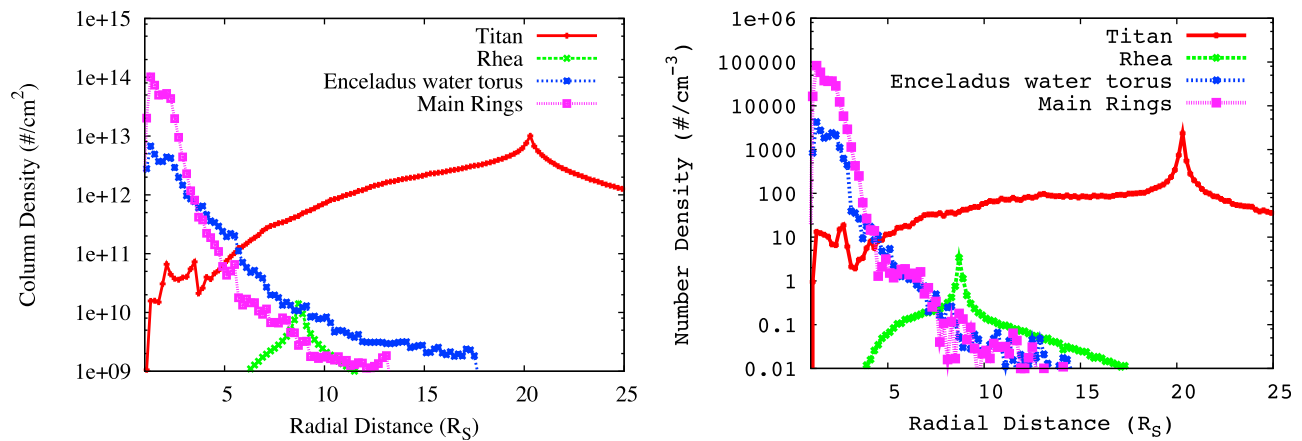


**Figure 2.** (left) Azimuthally averaged spatial morphology of the neutral  $H_2$  column density (number  $cm^{-2}$ ) as a function of distance from Saturn (in unit of Saturn's radius,  $R_S$ ). (right) The  $H_2$  number density (number  $cm^{-3}$ ) on the equatorial plane as a function of distance from Saturn (in unit of Saturn's radius,  $R_S$ ). Distributions due to each source: Titan (red), Rhea (green), Enceladus' water torus (blue), and main rings (pink).

Thomsen *et al.* [2010] that Titan is a major source for the  $H_2^+$  ions in the outer magnetosphere.

[26] The existence of an  $O_2$  cloud at Rhea [Martens *et al.*, 2008] was confirmed by the discovery of an  $O_2$  and  $CO_2$  atmosphere by the Cassini INMS measurements on the recent Rhea flyby in March 2010 [Teolis *et al.*, 2010]. Compared to  $H_2$ , most of  $O_2$  would remain gravitationally bound to Rhea because of its larger mass. The nondetection of an  $H_2$  atmosphere can be understood since about 80% of  $H_2$  coming out of Rhea's icy surface in thermal diffusion will directly escape. But those  $H_2$  are still bound in Saturn's gravity field contributing to a  $H_2$  torus. Our estimates of the source rate, which ignores the putative Rhea ring, show that the  $H_2$  from Rhea makes a relatively small contribution to the  $H_2$  in the middle magnetosphere which is immersed in the extended Titan torus. Since the results in Figure 2 are the azimuthally averaged distributions, there could be a much larger concentration of  $H_2$  close to Rhea ( $\sim 10^{12} cm^{-2}$  inside 2 Rhea radii).

[27] Our modeling of the  $H_2$  from Rhea, assuming a stoichiometry, is consistent with an  $O_2$  number density about a factor of two larger than the model based on the INMS observations for the R2 pass over Rhea's pole. This could be due to the average  $G$  value used or to the competition with  $CO_2$  formation in an ice containing carbonaceous material. However, the measured radiolytically produced neutral atmosphere is not consistent with the electron energy loss inside Rhea's Hill sphere ( $\sim 1.2 \times 10^{29} eV s^{-1}$ ) from R1 flyby (A. Rymer, private communication, 2010). Therefore, either the difference is due to the high variability, or the electron energy loss may be due to background E ring particles or Rhea's putative icy dust ring [Jones *et al.*, 2008]. This suggests that there could be an additional  $H_2/O_2$  source at a rate  $\sim 7 \times 10^{24} H_2 s^{-1}$  ( $G$  value 0.006  $H_2$  per 100 eV) which is comparable to that from Rhea's surface but would not significantly affect the INMS observations over Rhea's north pole.

[28] Between 3 and 6  $R_S$ , Enceladus contributes slightly more than half of  $H_2$  population using our estimates. The other part is provided by  $H_2$  scattered from the ring atmo-

sphere. Even though Enceladus has a huge water source rate, and is the major contributor of water group neutrals ( $H_2O$ ,  $OH$  and  $O$ ) to the Saturnian magnetosphere, most of the fragment  $H_2$  are dispersed significantly because of a large excess energy from photodissociation of water.

[29] It is clearly seen that there is also a prominent peak of  $H_2$  over the main rings. That is, when the  $H_2$  from any source impacts a ring particle it will thermally accommodate with the local surface temperature. Therefore,  $H_2$  accumulates over the main rings where it has a long lifetime:  $\sim 6 \times 10^8 s$  as compared to a few  $10^6$  seconds around 9  $R_S$ . The contribution to the  $H_2$  column density over the main rings from each contribution is also shown in Figure 2. The  $H_2$  accumulated over the main rings can be subsequently transported throughout the magnetosphere by charge exchange scattering with  $H_2^+$  ions and  $O_2^+$  ions over the main rings as well as with  $W^+$  ions in the inner region, as also described for the scattered  $O_2$  atmosphere of the main rings [Johnson *et al.*, 2006; Martens *et al.*, 2008; Tseng *et al.*, 2010]. To discuss the possible seasonal variations of the ring  $O_2$  atmosphere/ionosphere, Tseng *et al.* [2010] proposed that the  $O_2$  neutral (and  $O_2^+$  ion) source rates would be very small at Saturn's equinox if  $O_2$  is produced mainly by photolysis of the ring particles. However, Tseng and Ip [2011] also proposed that deposition of dissociation products from the Enceladus torus onto Saturn's A ring could mitigate this effect and could even be the dominant source of  $O_2$  over the main rings. Similarly, the seasonal variation of magnetospheric  $H_2$  (and  $H_2^+$ ) will differ from that for  $O_2$  since Titan is the dominant source of  $H_2$  outside of 6  $R_S$  and this source rate is likely insensitive to changes in the solar insolation angle. In spite of large uncertainties on each source rate, as discussed in section 2.1, it can be concluded that both the scattered component of ring  $H_2$  atmosphere and Enceladus' water torus make contributions in the  $H_2^+$  component of the magnetosphere inside  $\sim 6 R_S$ , while Titan plays a dominant role of  $H_2$  in the outer magnetosphere.

[30] Dissociation in the  $H_2$  ring's atmosphere contributes to those hydrogen atoms seen in the inner magnetosphere using the Cassini UVIS instrument [Shemansky *et al.*, 2009;

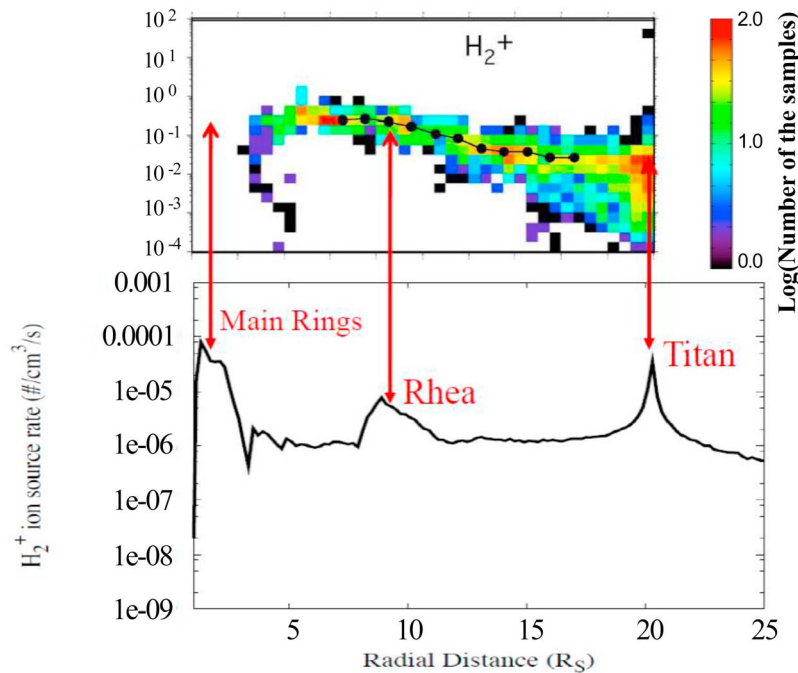


**Figure 3.** (top) The  $H_2^+$  ion density of CAPS observations within latitude of  $5^\circ$ . The black line with dots is the upper bound for the distribution of values. The number of sample measurements is indicated in color [Thomsen *et al.*, 2010, Figure 3b]. (bottom) The  $H_2^+$  ionization source rate at the equator (number  $\text{cm}^{-3} \text{s}^{-1}$ ) as a function of distance from Saturn (in unit of Saturn's radius,  $R_S$ ).

Melin *et al.*, 2009]. The spatial distribution of atomic hydrogen was shown to have a local time asymmetry, with the intensity increasing toward the top of Saturn's atmosphere. The density peak appeared on Saturn's sunlit hemisphere at  $\sim 13.5^\circ$  below the ring plane. Shemansky *et al.* [2009] suggested that neutral hydrogen flows outward from Saturn's sunlit hemisphere as a result of the electron impact dissociation of  $H_2$ . In steady state, H from photodissociation of  $H_2$  in the neutral cloud shown in Figure 2 would contribute  $\sim 1 \times 10^{35}$  atoms to the Saturn's neutral cloud. This is about a factor of 2 larger than the total hydrogen inside  $5 R_S$  observed by UVIS [Shemansky *et al.*, 2009]. Allowing for the uncertainty in the  $H_2$  ring atmosphere density, photodissociation of  $H_2$  over the main rings could, in principal, be an important contributor to the observed H density. However, the H from photodissociation are energetic having a large excess energy ( $\sim 60\%$  for 8.0 eV and  $\sim 40\%$  for 0.4 eV) [Huebner *et al.*, 1992] and are therefore dispersed throughout the magnetosphere as well as impacting Saturn's upper atmosphere. Since dynamic issues such as radiation pressure, loss to ring absorption, etc. need to be included, this source of H will be explored in a later study.

### 3.2. Spatial Distribution of $H_2^+$ Ion Source Rate

[31] Our model also gives the morphology of the  $H_2^+$  source rate in the magnetosphere. The  $H_2^+$  ions are produced from the neutral  $H_2$  cloud by photoionization, electron impact ionization and charge exchange with magnetospheric plasma ions ( $H^+$  and  $W^+$  in our model). Figure 3 shows the  $H_2^+$  ionization source rate (number  $\text{cm}^{-3} \text{s}^{-1}$ ) at the equator ( $\pm 0.1 R_S$ ) as a function of distance from Saturn ( $R_S$ ) (Figure 3, bottom), along with the  $H_2^+$  density distribution within lati-

tude =  $5^\circ$  from CAPS observations [Thomsen *et al.*, 2010, Figure 3b] (Figure 3, top). In the absence of diffusion, there are three prominent peaks in Figure 3 (bottom): main rings ( $\sim 6 \times 10^{-5} \text{ cm}^{-3} \text{ s}^{-1}$ ), around Rhea ( $\sim 7 \times 10^{-6} \text{ cm}^{-3} \text{ s}^{-1}$ ), and Titan ( $\sim 2 \times 10^{-5} \text{ cm}^{-3} \text{ s}^{-1}$ ). Even though the photoionization rate is small,  $\sim 9.2 \times 10^{-10} \text{ s}^{-1}$ , there is a large  $H_2^+$  ion source rate appears over the main rings because of accumulation of neutral  $H_2$  as described. The second peak located near Rhea's orbit resulted from the maximum electron impact ionization rate ( $\sim 1.7 \times 10^{-7} \text{ s}^{-1}$ ) around  $9 R_S$ . It corresponds to the location of maximum density and energy of hot electrons [Schippers *et al.*, 2008] and not to Rhea as a dominant source. Finally, a peak at Titan's orbit clearly indicates Titan is a major source of  $H_2^+$  ions in the outer magnetosphere.

### 3.3. $H_2^+$ Ion Densities

[32] It is difficult to simulate the spatial distribution of  $H_2^+$  ions throughout the Saturnian magnetosphere, since the ion loss rates vary with position in the magnetosphere and are dispersed primarily by rapid diffusion due to interchange instabilities which are highly variable. Hence, we compare the  $H_2^+$  ion source rates throughout the magnetosphere to the measured ion densities in Figure 3 and discuss the estimates of the ion lifetime below. However, over the main rings, the ion lifetime is primarily constrained by loss to ring particle absorption (a few  $10^4$  seconds for  $H_2^+$ ) allowing us to simulate the ion density distribution in this region of the magnetosphere. Hence, combining the source rate (shown in Figure 3) with the estimated lifetime, the  $H_2^+$  ion density over the main rings is estimated to be in the range of  $0.1 \text{ cm}^{-3}$  and  $1 \text{ cm}^{-3}$ . Except for the Cassini division, these values are generally consistent with the results of test

particle simulations of the H<sub>2</sub><sup>+</sup> ion density distribution as described in section 3.4.

[33] Since the hot tenuous plasma in the Saturnian magnetosphere is highly variable, and injection/interchange events occur frequently, there is considerable convective radial transport in Saturn's magnetosphere [Burch *et al.*, 2005; Hill *et al.*, 2005; Chen and Hill, 2008]. Therefore, the peaks in the source rate will be spread by diffusive-like processes. A plasma resident lifetime  $\sim 2$  days inside  $10 R_S$  is estimated by Chen *et al.* [2010]. Using this lifetime and the averaged ionization rate inside  $1 R_S$  of Rhea ( $\sim 5 \times 10^{-6} \text{ cm}^{-3} \text{ s}^{-1}$ ), the H<sub>2</sub><sup>+</sup> density near Rhea  $\sim 0.8 \text{ cm}^{-3}$ . This estimate is in rough agreement with the CAPS observations within latitude  $\sim 5^\circ$  shown in Figure 3 (top). Since new ions created near the equator move up and down the field lines, it is more useful to compare ion column densities. The observed H<sub>2</sub><sup>+</sup> ion column density near Rhea from CAPS observations is estimated to be  $\sim 4.7 \times 10^9 \text{ cm}^{-2}$  from  $N_i = n_i \times H_i$ , where  $n_i$  is ion number density and  $H_i$  is the H<sub>2</sub><sup>+</sup> scale height  $\sim 2.6 R_S$  [Thomsen *et al.*, 2010]. Using the neutral H<sub>2</sub> column density in our model multiplied by the averaged equatorial ionization rate ( $\sim 5 \times 10^{-6} \text{ cm}^{-3} \text{ s}^{-1}$ ) and the ion lifetime above, the H<sub>2</sub><sup>+</sup> ion column density is  $\sim 1.5 \times 10^{10} \text{ cm}^{-2}$ . This is roughly consistent with the CAPS observations.

[34] Titan mostly orbits inside the average location of Saturn's magnetopause but at times it interacts directly with the solar wind or the magnetosheath plasma. Cassini confirmed that Titan's orbit is in a particularly complex and unstable plasma environment [Arridge *et al.*, 2008; Jackman *et al.*, 2008; Hill *et al.*, 2008; Russell *et al.*, 2008; Rymer *et al.*, 2009 and references therein]. The plasma can be added to or lost from its magnetosphere through interchange instability, injection events, plasma bubble penetrations, and magnetotail reconnections, etc. These are mostly associated with the periodicities within about one magnetospheric rotation period  $\sim 10.7$  h [Arridge *et al.*, 2008; Russell *et al.*, 2008; Burch *et al.*, 2008]. Using one half of the rotation period as an average lifetime and the ionization rate averaged inside  $1 R_S$  of Titan's orbit ( $\sim 7 \times 10^{-6} \text{ cm}^{-3} \text{ s}^{-1}$ ), the H<sub>2</sub><sup>+</sup> ion density is estimated to be  $\sim 0.13 \text{ cm}^{-3}$ , which is higher than the typical H<sub>2</sub><sup>+</sup> density near equator observed by CAPS ( $\sim 0.02 \text{ cm}^{-3}$ ) (e.g., Figure 3). A better comparison is the H<sub>2</sub><sup>+</sup> ion column density. Again using half the rotation period, we estimate this to be  $\sim 1.2 \times 10^9 \text{ cm}^{-2}$  which is seen to be in rough agreement with the CAPS observations ( $n_i \times H_i = 0.02 \times 5 \times 10^{10} \sim 0.9 \times 10^9 \text{ cm}^{-2}$ ). We note that both at Rhea and Titan using the smaller H<sub>2</sub> source rate suggested by Strobel [2008] would produce better agreement with the averaged CAPS data.

### 3.4. H<sub>2</sub><sup>+</sup> Density Distribution Over Main Rings: Comparison to CAPS Data

[35] To simulate the steady state distribution of H<sub>2</sub><sup>+</sup> over the main rings, the total integration time is  $\sim 1 \times 10^6$  s since the ions are rapidly lost to ring absorption in a short time, approximately a few  $10^4$  seconds. In our model H<sub>2</sub><sup>+</sup> is formed primarily by photoionization of H<sub>2</sub> at a rate  $K_i = 9.2 \times 10^{-10} \text{ s}^{-1}$ . In the ring shadow zone the ionization rate is reduced by a factor of  $\exp(-\tau/\cos \gamma)$ . Each new H<sub>2</sub><sup>+</sup> ion is formed with the local Keplerian velocity plus the thermal velocity in a random direction. The equation of motion of the ions is determined by the gravitational force and the Lorentz

force,  $mdV/dt = -GM/r^2 + q[E + V \times B]$  where  $V$  is the ion velocity and  $E$  is the corotational electric field at pickup, given by  $E = V_{CO} \times B$ , where  $V_{CO}$  is the corotational velocity and  $B$  is the local magnetic field.  $B$  is treated as a dipole field with a northward shift of  $0.04 R_S$  [Connerney *et al.*, 1983]. The ions are scattered by interaction with the neutrals (as described in section 3.3) and are lost to ring absorption and to precipitation into Saturn's upper atmosphere. Because of the low electron density, recombination is ignored. The detail description of our model of the ring H<sub>2</sub><sup>+</sup> ionosphere is like that for O<sub>2</sub><sup>+</sup> in the work of Tseng *et al.* [2010].

[36] The azimuthally symmetric spatial distribution of H<sub>2</sub><sup>+</sup> ring ionosphere simulated for the SOI pass over the main rings discussed above is shown in Figure 4. This assumes photolytic decomposition of ice as the leading formation of H<sub>2</sub>. Fewer H<sub>2</sub><sup>+</sup> ions are found above the ring plane since photoionization is the leading ion formation process and the ring shadow effect is taken into account in our model. In addition, as a result of the vertical shift of Saturn's magnetic equator ( $Z = +0.04 R_S$ ) and of Saturn's gravity, the ion motion can be skewed. The most obvious asymmetric pattern above and below the ring plane is located inside the B ring because of its large optical thickness. It is also clearly seen in Figure 4 that, inside the radius ( $\sim 1.7 R_S$ ), H<sub>2</sub><sup>+</sup> ions primarily precipitate into Saturn's southern hemisphere because of Saturn's gravity. These effects have been explored for the O<sub>2</sub><sup>+</sup> ring ionosphere [e.g., Tseng *et al.*, 2010]. There is a density enhancement with a maximum value of  $\sim 180 \text{ cm}^{-3}$  in the Cassini division due to the reduced optical thickness, hence, reduced ring particle absorption in our model. Compared to the O<sub>2</sub><sup>+</sup> ring ionosphere [e.g., Tseng *et al.*, 2010, Figure 4a], the H<sub>2</sub><sup>+</sup> density near the ring plane is at least 1 order of magnitude smaller as a result of one tenth smaller H<sub>2</sub> photoionization rate and a higher loss rate to ring absorption. In addition, the H<sub>2</sub><sup>+</sup> ring ionosphere appears much more extended than O<sub>2</sub><sup>+</sup> especially in Cassini division and over the A ring. This is a mass effect resulting in H<sub>2</sub><sup>+</sup> (H<sub>2</sub>) forming with a larger scale height and a larger initial thermal velocity ( $\sim 4$  times of O<sub>2</sub><sup>+</sup> (H<sub>2</sub>)) [e.g., Johnson *et al.*, 2006]. The mass effect can be also seen in an enhancement of the density ratio of H<sub>2</sub><sup>+</sup> to O<sub>2</sub><sup>+</sup> appearing in the Cassini division shown in Figure 5. Because the absolute values can be underestimated, as discussed in section 2.1, we show the spatial distribution of the density ratio of H<sub>2</sub><sup>+</sup> to O<sub>2</sub><sup>+</sup> along the Cassini spacecraft trajectory at SOI in Figure 5. The solid line shown in Figure 5 is with the model O<sub>2</sub><sup>+</sup> density from Tseng *et al.* [2010] with H<sub>2</sub> and O<sub>2</sub> presumed to be formed in a stoichiometric ratio of 2 to 1, while the dashed line uses the density inferred from the CAPS O<sub>2</sub><sup>+</sup> data [Tokar *et al.*, 2005]. Figure 5 implies that there is a disagreement ( $\sim$  a factor of 10) between the model O<sub>2</sub><sup>+</sup> density and the CAPS O<sub>2</sub><sup>+</sup> data over the B ring. It might be attributed to recycling as discussed earlier or be related to electrostatic charging of the ring plane [Ip, 1984]. In addition we note that, CAPS should have detected H<sub>2</sub><sup>+</sup> in Cassini division if H<sub>2</sub> and O<sub>2</sub> are formed stoichiometrically. Although CAPS reported a nondetection of H<sub>2</sub><sup>+</sup> over the main rings at SOI [Young *et al.*, 2005; Tokar *et al.*, 2005], a recent reinvestigation shows that it is possible for the H<sub>2</sub><sup>+</sup> signals to be hidden in the high-energy tail of O<sup>+</sup> (R. L. Tokar, private communication, 2010). Either nondetection (an upper limit)

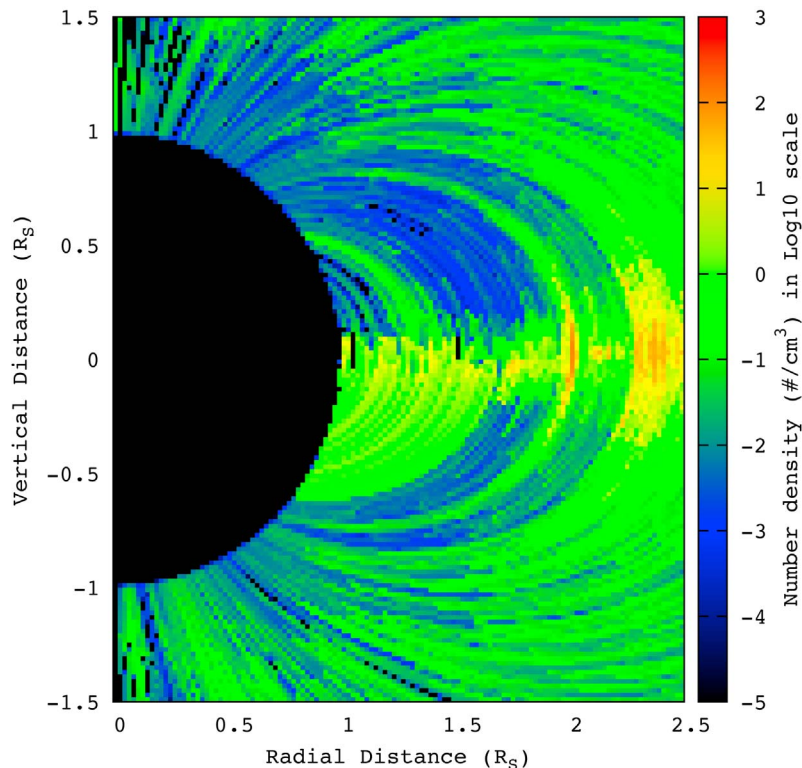


**Figure 4.** The H<sub>2</sub><sup>+</sup> ion density distribution over the main rings in two dimensions with an azimuthal average:  $x$  axis, distance from Saturn;  $y$  axis, vertical distance from orbital plane (both in unit of  $R_S$ ). Color bar indicates the H<sub>2</sub><sup>+</sup> ion number density in log 10 scale.

or detection of H<sub>2</sub><sup>+</sup> can be used to constrain the O<sub>2</sub>/H<sub>2</sub> source rate from main rings, since recycling could play an important role as discussed in section 2.1.

[37] Recycling of oxygen can enhance the O<sub>2</sub> source rate over the main rings by a factor of 5–10. This can occur by ring absorption of the photolytic products of O<sub>2</sub> (O, O<sup>+</sup> and O<sub>2</sub><sup>+</sup>) [Johnson *et al.*, 2006; Tseng *et al.*, 2010]. Moreover, a large portion (~30%) of Enceladus’ outgassed water and its fragments may be impinging onto the A ring [Jurac and Richardson, 2007; Farrell *et al.*, 2008; Cassidy and Johnson, 2010]. These molecular fragments and ions can react to form neutral O<sub>2</sub>/H<sub>2</sub> via grain surface chemistry and act as an important “exogenic” supplier for the ring atmosphere [Tseng and Ip, 2011] and as suggested by recent experiments [Cooper *et al.*, 2010]. In addition, the H<sup>+</sup> flowing out of Saturn’s ionosphere [Waite, 1981] and the hydrogen atoms escaping from Saturn’s upper atmosphere [Shemansky *et al.*, 2009] can also react on the ring particle surfaces contributing to the ring atmosphere. The thesis of recycling of the products of the ejected O<sub>2</sub>/H<sub>2</sub> needs further analysis.

#### 4. Summary

[38] In this paper we carried out the simulations of the spatial morphology of the Saturn’s H<sub>2</sub> cloud and of the H<sub>2</sub><sup>+</sup> ion source rates. We show how H<sub>2</sub> and, hence, H<sub>2</sub><sup>+</sup> is distributed throughout the magnetosphere from sources over the main rings, Enceladus, Rhea and Titan. We also estimated the density distribution of the ring H<sub>2</sub><sup>+</sup> ionosphere.

[39] 1. The neutral H<sub>2</sub> lifetime is largest,  $\sim 6 \times 10^8$  s, over the main rings because the energetic plasma is absorbed by ring particles so that photolytic reactions dominate. The H<sub>2</sub> lifetime reaches its minimum, approximately a few  $10^6$  seconds, around  $9 R_S$  as a result of the large ionization rate due to the peak in the hot electron density and temperature. This results in a peak H<sub>2</sub><sup>+</sup> ion source rate around  $9 R_S$  in our

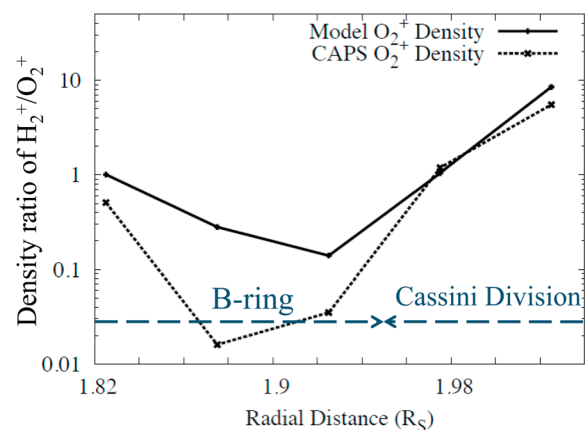


**Figure 5.** The density ratio of H<sub>2</sub><sup>+</sup> to O<sub>2</sub><sup>+</sup> along the Cassini trajectory at SOI. The solid line is O<sub>2</sub><sup>+</sup> density from Tseng *et al.* [2010] assuming H<sub>2</sub> and O<sub>2</sub> are produced in a stoichiometry ratio of 2:1. The dashed line is O<sub>2</sub><sup>+</sup> density from CAPS data [Tokar *et al.*, 2005]. The  $x$  axis is the radial distance from Saturn ( $R_S$ ).

model (shown in Figure 3). This is not attributed to a large source rate at Rhea, but to a combination of increasing electron temperature and a peak density of suprathermal electron around Rhea [Schipper *et al.*, 2008].

[40] 2. The H<sub>2</sub> column density over the main rings is largest because thermal accommodation of H<sub>2</sub> with the ring particles produces slow H<sub>2</sub> with long lifetimes so it can accumulate. The scattered component of ring H<sub>2</sub> atmosphere and Enceladus' water torus are the primary sources of H<sub>2</sub> inside ~6.0 R<sub>S</sub>, while Titan is the dominant source in the outer magnetosphere.

[41] 3. Using the estimated plasma residence time of ~2 days [Chen *et al.*, 2010], the H<sub>2</sub><sup>+</sup> ion column density is estimated to be ~1.5 × 10<sup>10</sup> cm<sup>-2</sup> around Rhea, which is roughly consistent with the CAPS result [Thomsen *et al.*, 2010]. If we assume approximately one half of the Saturn rotation period as the average lifetime at Titan's orbit, we obtain a H<sub>2</sub><sup>+</sup> ion column density of ~1.2 × 10<sup>9</sup> cm<sup>-2</sup> which is also in agreement with the CAPS data [Thomsen *et al.*, 2010].

[42] 4. Although the H<sub>2</sub><sup>+</sup> density is smaller than the O<sub>2</sub><sup>+</sup> density over the main rings, an enhancement in the density ratio of H<sub>2</sub><sup>+</sup> to O<sub>2</sub><sup>+</sup> is predicted in the Cassini division, if H<sub>2</sub> and O<sub>2</sub> are formed in a stoichiometric ratio of two to one (Figure 5). This is such that CAPS should have detected H<sub>2</sub><sup>+</sup> in this region at SOI. Hence, the reinvestigation of CAPS data or future observations can give us an important constraint on the source mechanism and recycling effects.

[43] **Acknowledgments.** We thank H. T. Smith and A. Rymer for useful discussions and comments. This work is supported by a grant from NASA's Planetary Atmosphere's Program and by a NASA Cassini data analysis grant. Work at Los Alamos was conducted under the auspices of the U.S. Department of Energy with funding from NASA's Cassini project.

[44] Masaki Fujimoto thanks the reviewers for their assistance in evaluating this paper.

## References

- Arridge, C. S., N. André, N. Achilleos, K. K. Khurana, C. L. Bertucci, L. K. Gilbert, G. R. Lewis, A. J. Coates, and M. K. Dougherty (2008), Thermal electron periodicities at 20 R<sub>S</sub> in Saturn's magnetosphere, *Geophys. Res. Lett.*, *35*, L15107, doi:10.1029/2008GL034132.
- Bouhram, M., R. E. Johnson, J.-J. Berthelier, J.-M. Illiano, R. L. Tokar, D. T. Young, and F. J. Crary (2006), A test-particle model of the atmosphere/ionosphere system of Saturn's main rings, *Geophys. Res. Lett.*, *33*, L05106, doi:10.1029/2005GL025011.
- Broadfoot, A. L., et al. (1981), Extreme ultraviolet observations from Voyager 1 encounter with Saturn, *Science*, *212*, 206–211, doi:10.1126/science.212.4491.206.
- Burch, J. L., J. Goldstein, T. W. Hill, D. T. Young, F. J. Crary, A. J. Coates, N. André, W. S. Kurth, and E. C. Sittler Jr. (2005), Properties of local plasma injections in Saturn's magnetosphere, *Geophys. Res. Lett.*, *32*, L14S02, doi:10.1029/2005GL022611.
- Burch, J. L., J. Goldstein, P. Mokashi, W. S. Lewis, C. Paty, D. T. Young, A. J. Coates, M. K. Dougherty, and N. André (2008), On the cause of Saturn's plasma periodicity, *Geophys. Res. Lett.*, *35*, L14105, doi:10.1029/2008GL034951.
- Cassidy, T. A., and R. E. Johnson (2010), Collisional spreading of Enceladus' neutral cloud, *Icarus*, *209*, 696–703, doi:10.1016/j.icarus.2010.04.010.
- Chen, Y., and T. W. Hill (2008), Statistical analysis of injection/dispersion events in Saturn's inner magnetosphere, *J. Geophys. Res.*, *113*, A07215, doi:10.1029/2008JA013166.
- Chen, Y., T. W. Hill, A. M. Rymer, and R. J. Wilson (2010), Rate of radial transport of plasma in Saturn's inner magnetosphere, *J. Geophys. Res.*, *115*, A10211, doi:10.1029/2010JA015412.
- Connerney, J. E. P., M. H. Acuna, and N. F. Ness (1983), Currents in Saturn's magnetosphere, *J. Geophys. Res.*, *88*, 8779–8789, doi:10.1029/JA088iA11p08779.
- Cui, J., R. V. Yelle, and K. Volk (2008), Distribution and escape of molecular hydrogen in Titan's thermosphere and exosphere, *J. Geophys. Res.*, *113*, E10004, doi:10.1029/2007JE003032.
- Danby, J. M. A. (1989), *Fundamentals of Celestial Mechanics*, Willmann-Bell, Richmond, Va.
- De La Haye, V., et al. (2007), Cassini ion and neutral mass spectrometer data in Titan's upper atmosphere and exosphere: Observation of a suprathermal corona, *J. Geophys. Res.*, *112*, A07309, doi:10.1029/2006JA012222.
- Dialynas, K., S. M. Krimigis, D. G. Mitchell, D. C. Hamilton, N. Krupp, and P. C. Brandt (2009), Energetic ion spectral characteristics in the Saturnian magnetosphere using Cassini/MIMI measurements, *J. Geophys. Res.*, *114*, A01212, doi:10.1029/2008JA013761.
- Cooper, P., N. Do, A. Strube, and L. Ammann (2010), Oxidant loading of icy satellite surfaces by re-deposition and subsequent surface chemistry, paper presented at 42nd Annual Meeting, Div. for Planet. Sci., Am. Astron. Soc., Pasadena, Calif.
- Eposito, L. W., J. E. Colwell, and K. Larsen (2005), Ultraviolet imaging spectroscopy shows an active Saturnian system, *Science*, *307*, 1251–1255, doi:10.1126/science.1105606.
- Famá, M., J. Shi, and R. A. Baragiola (2008), Sputtering of ice by low-energy ions, *Surf. Sci.*, *602*, 156–161, doi:10.1016/j.susc.2007.10.002.
- Farmer, A. J. (2009), Saturn in hot water: Viscous evolution of the Enceladus torus, *Icarus*, *202*, 280–286, doi:10.1016/j.icarus.2009.02.031.
- Farrell, W. M., M. L. Kaiser, D. A. Gurnett, W. S. Kurth, A. M. Persoon, J. E. Wahlund, and P. Canu (2008), Mass unloading along the inner edge of the Enceladus plasma torus, *Geophys. Res. Lett.*, *35*, L02203, doi:10.1029/2007GL032306.
- Hansen, C. J., et al. (2006), Enceladus' water vapor plume, *Science*, *311*, 1422–1425, doi:10.1126/science.1121254.
- Hasted, J. B. (1972), *Physics of Atomic Collisions*, 2nd ed., Elsevier, New York.
- Hill, T. W., A. M. Rymer, J. L. Burch, F. J. Crary, D. T. Young, M. F. Thomsen, D. Delapp, N. André, A. J. Coates, and G. R. Lewis (2005), Evidence for rotationally driven plasma transport in Saturn's magnetosphere, *Geophys. Res. Lett.*, *32*, L14S10, doi:10.1029/2005GL022620.
- Hill, T. W., et al. (2008), Plasmoids in Saturn's magnetotail, *J. Geophys. Res.*, *113*, A01214, doi:10.1029/2007JA012626.
- Huebner, W. F., J. J. Keady, and S. P. Lyon (1992), Solar photo rates for planetary atmospheres and atmospheric pollutants, *Astrophys. Space Sci.*, *195*, 1–294, doi:10.1007/BF00644558.
- Ip, W.-H. (1984), Electrostatic charging of the rings of Saturn: A parameter study, *J. Geophys. Res.*, *89*, 3829–3836, doi:10.1029/JA089iA06p03829.
- Ip, W.-H. (1995), The exospheric systems of Saturn's rings, *Icarus*, *115*, 295–303, doi:10.1006/icar.1995.1098.
- Ip, W.-H. (1997), On the neutral cloud distribution in the Saturnian magnetosphere, *Icarus*, *126*, 42–57, doi:10.1006/icar.1996.5618.
- Ip, W.-H. (2005), An update on the ring exosphere and plasma disc of Saturn, *Geophys. Res. Lett.*, *32*, L13204, doi:10.1029/2004GL022217.
- Jackman, C. M., et al. (2008), A multi-instrument view of tail reconnection at Saturn, *J. Geophys. Res.*, *113*, A11213, doi:10.1029/2008JA013592.
- Johnson, R. E. (1981), *Introduction to Atomic and Molecular Collisions*, Plenum, New York.
- Johnson, R. E. (1990), *Energetic Charged Particle Interactions With Atmospheres and Surfaces*, Springer, Berlin. (Available at <http://people.virginia.edu/~rej/book.html>)
- Johnson, R. E. (2009), Sputtering and heating of Titan's upper atmosphere, *Philos. Trans. R. Soc. A*, *367*, 753–771, doi:10.1098/rsta.2008.0244.
- Johnson, R. E. (2011), Photolysis and radiolysis of water ice, in *Physics and Chemistry at Low Temperatures*, edited by L. Khriachtchev, World Sci., Singapore, in press.
- Johnson, R. E., J. W. Boring, J. W. Garrett, C. Reimann, L. J. Lanzerotti, and W. L. Brown (1982), Charged particle erosion of the icy satellites of Jupiter and Saturn, *Bull. Am. Astron. Soc.*, *14*, 745.
- Johnson, R. E., R. W. Carlson, J. F. Cooper, C. Paranicas, M. H. Moore, and M. C. Wong (2004), Radiation Effects on the Surface of the Galilean Satellites, in *Jupiter—The Planet, Satellites and Magnetosphere*, edited by F. Bagenal, T. Dowling, and W. B. McKinnon, chap. 20, pp. 485–512, Cambridge Univ., Cambridge, U. K.
- Johnson, R. E., et al. (2006), Production, ionization and redistribution of O<sub>2</sub> in Saturn's ring atmosphere, *Icarus*, *180*, 393–402, doi:10.1016/j.icarus.2005.08.021.
- Johnson, R. E., M. Famá, M. Liu, R. A. Baragiola, E. C. Sittler, and H. T. Smith (2008), Sputtering of ice grains and icy satellites in Saturn's inner magnetosphere, *Planet. Space Sci.*, *56*, 1238–1243, doi:10.1016/j.pss.2008.04.003.
- Johnson, R. E., O. J. Tucker, M. Michael, E. C. Sittler, H. T. Smith, D. T. Young, and J. H. Waite (2009), Mass loss processes in Titan's upper

- atmosphere, in *Titan From Cassini-Huygens*, chap. 15, pp. 373–391, Springer, New York.
- Jones, G. H., et al. (2008), The dust halo of Saturn's largest icy moon, Rhea, *Science*, *319*, 1380–1384, doi:10.1126/science.1151524.
- Jurac, S., and J. D. Richardson (2005), A self-consistent model of plasma and neutrals at Saturn: Neutral cloud morphology, *J. Geophys. Res.*, *110*, A09220, doi:10.1029/2004JA010635.
- Jurac, S., and J. D. Richardson (2007), Neutral cloud interaction with Saturn's main rings, *Geophys. Res. Lett.*, *34*, L08102, doi:10.1029/2007GL029567.
- Jurac, S., R. E. Johnson, and J. D. Richardson (2001), Saturn's E ring and production of the neutral torus, *Icarus*, *149*, 384–396, doi:10.1006/icar.2000.6528.
- Jurac, S., M. A. McGrath, R. E. Johnson, J. D. Richardson, V. M. Vasyliunas, and A. Eviatar (2002), Saturn: Search for a missing water source, *Geophys. Res. Lett.*, *29*(24), 2172, doi:10.1029/2002GL015855.
- Lebonnois, S., E. L. O. Bakes, and C. P. McKay (2003), Atomic and molecular hydrogen budget in Titan's atmosphere, *Icarus*, *161*, 474–485, doi:10.1016/S0019-1035(02)00039-8.
- Luhmann, J. G., R. E. Johnson, R. L. Tokar, S. A. Ledvina, and T. E. Cravens (2006), A model of the ionosphere of Saturn's rings and its implications, *Icarus*, *181*, 465–474, doi:10.1016/j.icarus.2005.11.022.
- Martens, H. R., D. B. Reisenfeld, J. D. Williams, R. E. Johnson, and H. T. Smith (2008), Observations of molecular oxygen ions in Saturn's inner magnetosphere, *Geophys. Res. Lett.*, *35*, L20103, doi:10.1029/2008GL035433.
- Melin, H., D. E. Shemansky, and X. Liu (2009), The distribution of atomic hydrogen and oxygen in the magnetosphere of Saturn, *Planet. Space Sci.*, *57*, 1743–1753, doi:10.1016/j.pss.2009.04.014.
- Michael, M., R. E. Johnson, F. Leblanc, M. Liu, J. G. Luhmann, and V. I. Shematovich (2005), Ejection of nitrogen from Titan's atmosphere by magnetospheric ions and pick-up ions, *Icarus*, *175*, 263–267, doi:10.1016/j.icarus.2004.11.004.
- Persoon, A. M., et al. (2009), A diffusive equilibrium model for the plasma density in Saturn's magnetosphere, *J. Geophys. Res.*, *114*, A04211, doi:10.1029/2008JA013912.
- Porco, C. C., et al. (2006), Cassini observes the active south pole of Enceladus, *Science*, *311*, 1393–1401, doi:10.1126/science.1123013.
- Pospieszalska, M. K., and R. E. Johnson (1989), Magnetospheric ion bombardment profiles of satellites—Europa and Dione, *Icarus*, *78*, 1–13, doi:10.1016/0019-1035(89)90065-1.
- Russell, C. T., C. M. Jackman, H. Y. Wei, C. Bertucci, and M. K. Dougherty (2008), Titan's influence on Saturnian substorm occurrence, *Geophys. Res. Lett.*, *35*, L12105, doi:10.1029/2008GL034080.
- Rymer, A. M., et al. (2007), Electron source in Saturn's magnetosphere, *J. Geophys. Res.*, *112*, A02201, doi:10.1029/2006JA012017.
- Rymer, A. M., H. T. Smith, A. Wellbrock, A. J. Coates, and D. T. Young (2009), Discrete classification and electron energy spectra of Titan's varied magnetospheric environment, *Geophys. Res. Lett.*, *36*, L15109, doi:10.1029/2009GL039427.
- Schippers, P., et al. (2008), Multi-instrument analysis of electron populations in Saturn's magnetosphere, *J. Geophys. Res.*, *113*, A07208, doi:10.1029/2008JA013098.
- Shemansky, D. E., and D. T. Hall (1992), The distribution of atomic hydrogen in the magnetosphere of Saturn, *J. Geophys. Res.*, *97*, 4143–4161, doi:10.1029/91JA02805.
- Shemansky, D. E., P. Matheson, D. T. Hall, H.-Y. Hu, and T. M. Tripp (1993), Detection of the hydroxyl radical in the Saturn magnetosphere, *Nature*, *363*, 329–331, doi:10.1038/363329a0.
- Shemansky, D. E., X. Liu, and H. Melin (2009), The Saturn hydrogen plume, *Planet. Space Sci.*, *57*, 1659–1670, doi:10.1016/j.pss.2009.05.002.
- Sittler, E. C., et al. (2008), Ion and neutral sources and sinks within Saturn's inner magnetosphere: Cassini results, *Planet. Space Sci.*, *56*, 3–18, doi:10.1016/j.pss.2007.06.006.
- Smith, H. T., R. E. Johnson, M. E. Perry, D. G. Mitchell, R. L. McNutt, and D. T. Young (2010), Enceladus plume variability and the neutral gas densities in Saturn's magnetosphere, *J. Geophys. Res.*, *115*, A10252, doi:10.1029/2009JA015184.
- Strobel, D. F. (2008), Titan's hydrodynamically escaping atmosphere, *Icarus*, *193*, 588–594, doi:10.1016/j.icarus.2007.08.014.
- Tawara, H., T. Kato, and Y. Nakai (1985), Cross sections for electron capture and loss by positive ions in collisions with atomic and molecular hydrogen, *At. Data Nucl. Data Tables*, *32*, 235, doi:10.1016/0092-640X(85)90007-5.
- Teolis, B. D., et al. (2010), Cassini finds an oxygen–carbon dioxide atmosphere at Saturn's icy moon Rhea, *Science*, *330*, 1813–1815, doi:10.1126/science.1198366.
- Thomsen, M. F., D. B. Reisenfeld, D. M. Delapp, R. L. Tokar, D. T. Young, F. J. Crary, E. C. Sittler, M. A. McGraw, and J. D. Williams (2010), Survey of ion plasma parameters in Saturn's magnetosphere, *J. Geophys. Res.*, *115*, A10220, doi:10.1029/2010JA015267.
- Tokar, R. L., et al. (2005), Cassini observations of the thermal plasma in the vicinity of Saturn's main rings and the F and G rings, *Geophys. Res. Lett.*, *32*, L14S04, doi:10.1029/2005GL022690.
- Tseng, W.-L., and W.-H. Ip (2011), An assessment and test of Enceladus as an important source of Saturn's ring atmosphere and ionosphere, *Icarus*, doi:10.1016/j.icarus.2010.12.003, in press.
- Tseng, W.-L., W.-H. Ip, R. E. Johnson, T. A. Cassidy, and M. K. Elrod (2010), The structure and time variability of the ring atmosphere and ionosphere, *Icarus*, *206*, 382–389, doi:10.1016/j.icarus.2009.05.019.
- Tucker, O. J., and R. E. Johnson (2009), Thermally driven atmospheric escape: Monte Carlo simulations for Titan's atmosphere, *Planet. Space Sci.*, *57*, 1889–1894, doi:10.1016/j.pss.2009.06.003.
- Waite, J. H., Jr. (1981), The ionosphere of Saturn, Ph.D. thesis, Univ. of Michigan, Ann Arbor.
- Waite, J. H., Jr., et al. (2005), Oxygen ions observed near Saturn's A ring, *Science*, *307*, 1260–1262, doi:10.1126/science.1105734.
- Waite, J. H., Jr., et al. (2006), Cassini ion and neutral mass spectrometer: Enceladus plume composition and structure, *Science*, *311*, 1419–1422, doi:10.1126/science.1121290.
- Wilson, R. J., R. L. Tokar, M. G. Henderson, T. W. Hill, M. F. Thomsen, and D. H. Pontius (2008), Cassini plasma spectrometer thermal ion measurements in Saturn's inner magnetosphere, *J. Geophys. Res.*, *113*, A12218, doi:10.1029/2008JA013486.
- Yelle, R. V., J. Cui, and I. C. F. Müller-Wodarg (2008), Methane escape from Titan's atmosphere, *J. Geophys. Res.*, *113*, E10003, doi:10.1029/2007JE003031.
- Yoon, J.-S., M.-Y. Song, J.-M. Han, S. H. Hwang, W.-S. Chang, B. Lee, and Y. Itikawa (2008), Cross sections for electron collisions with hydrogen molecules, *J. Phys. Chem. Ref. Data*, *37*(2), 913–931.
- Young, D. T., et al. (2005), Composition and dynamics of plasma in Saturn's magnetosphere, *Science*, *307*, 1262–1266, doi:10.1126/science.1106151.

T. A. Cassidy, Jet Propulsion Laboratory, Pasadena, CA 91109, USA.  
 M. K. Elrod, R. E. Johnson, and W.-L. Tseng, Materials Science and Engineering Department, University of Virginia, Charlottesville, VA 22903, USA. (wt7b@virginia.edu)  
 M. F. Thomsen, Los Alamos National Laboratory, Los Alamos, NM 87545, USA.